2D 1H and 3D 1H-15N NMR of zinc-rubredoxins: Contributions of the β-sheet to thermostability

ARTICLE *in* PROTEIN SCIENCE · MAY 2008

Impact Factor: 2.85 · DOI: 10.1002/pro.5560050510 · Source: PubMed

Protein Science (1996), *5*:883–894. Cambridge University Press. Printed in the USA.

2D ^{1}H and 3D ^{1}H-^{15}N NMR of zinc-rubredoxins: Contributions of the β-sheet to thermostability

KIMBERLY A. RICHIE, QUINCY TENG, CHRISTOPHER J. ELKIN, AND DONALD M. KURTZ, JR.

Department of Chemistry and Center for Metalloenzyme Studies, University of Georgia, Athens, Georgia 30602

(RECEIVED December 5, 1995; ACCEPTED February 6, 1996)

Abstract

Based on 2D ^{1}H-^{1}H and 2D and 3D ^{1}H-^{15}N NMR spectroscopies, complete ^{1}H NMR assignments are reported for zinc-containing *Clostridium pasteurianum* rubredoxin (Cp ZnRd). Complete ^{1}H NMR assignments are also reported for a mutated Cp ZnRd, in which residues near the N-terminus, namely, Met 1, Lys 2, and Pro 15, have been changed to their counterparts, (−), Ala and Glu, respectively, in rubredoxin from the hyperthermophilic archaeon, *Pyrococcus furiosus* (Pf Rd). The secondary structure of both wild-type and mutated Cp ZnRds, as determined by NMR methods, is essentially the same. However, the NMR data indicate an extension of the three-stranded β-sheet in the mutated Cp ZnRd to include the N-terminal Ala residue and Glu 15, as occurs in Pf Rd. The mutated Cp Rd also shows more intense NOE cross peaks, indicating stronger interactions between the strands of the β-sheet and, in fact, throughout the mutated Rd. However, these stronger interactions do not lead to any significant increase in thermostability, and both the mutated and wild-type Cp Rds are much less thermostable than Pf Rd. These correlations strongly suggest that, contrary to a previous proposal [Blake PR et al., 1992, *Protein Sci 1*:1508–1521], the thermostabilization mechanism of Pf Rd is *not* dominated by a unique set of hydrogen bonds or electrostatic interactions involving the N-terminal strand of the β-sheet. The NMR results also suggest that an overall tighter protein structure does not necessarily lead to increased thermostability.

Keywords: *Clostridium pasteaurianum*; 2D NMR; 3D NMR; mutated rubredoxin; protein secondary structure; protein thermostability; rubredoxin; zinc-containing rubredoxin

The group of bacterial and archaeal iron–sulfur proteins known as rubredoxins appears to be ideal for delineating molecular determinants of non-heme metalloprotein structure, thermostability, and redox properties. Rds have in common the following favorable characteristics for such investigations: small size (typically 52–54 residues), a very simple redox active $Fe(SCys)_4$ site (whose Cys residues are underlined in Scheme 1), a large and continually expanding database of amino acid sequences (Zeng et al., 1995), at least five high-resolution X-ray crystal structures (Sieker et al., 1994), a characteristic structural motif featuring a three-stranded β-sheet, and well-characterized proteins from several mesophiles and from the hyperthermophilic archaeon *Pyrococcus furiosus*. Pf Rd is known to be remarkably thermostable compared to Rds from mesophilic organisms (Blake et al., 1991; Day et al., 1992). However, there are no obvious distinguishing structural or spectroscopic features of the FeS_4 site in Pf Rd compared to Rds from mesophiles. Instead, based on the NMR solution structure of the zinc-substituted Pf Rd (Blake et al., 1992) and the X-ray crystal structure of Pf FeRd (Day et al., 1992), a unique set of hydrogen bonds and electrostatic interactions was proposed to inhibit "unzipping" of the three-stranded β-sheet at high temperatures. This inhibition could be the dominant mechanism for thermal stabilization of the hyperthermophilic Rd relative to mesophilic Rds (cf. Adams & Kelly, 1995 for a more recent discussion of this issue).

Reprint requests to: Donald M. Kurtz, Jr., Department of Chemistry, University of Georgia, Athens, Georgia 30602; e-mail: kurtz@bscr.uga.edu.

Abbreviations: Rd, rubredoxin; Cp, *Clostridium pasteurianum*; M1(−)K2AP15E Cp Rd, Met 1 → (−), Lys 2 → Ala,Pro 15 → Glu triply mutated Cp Rd; Pf, *Pyrococcus furiosus*; 2D, two-dimensional; 3D, three-dimensional; Tris-HCl, tris(hydroxymethyl)aminomethane-hydrochloride; HEPES, *N*-(hydroxyethyl)piperazine-*N*′-2-ethanesulfonic acid; HSQC, heteronuclear single-quantum coherence; ICP-AE, inductively coupled plasma-atomic emission; OD_{600}, optical density measured at 600 nm; IPTG, isopropyl-β-D-thiogalactopyranoside; NOESY, nuclear Overhauser effect spectroscopy; DIPSI, decoupling in the presence of scalar interactions; DQF-COSY, double quantum-filtered correlation spectroscopy; SCUBA, stimulated cross peaks under bleached alphas; DDS, 2,2-dimethyl-2-silapentane-5-sulfonate; TOCSY, total correlation spectroscopy.

Scheme 1

```
          1        10        20        30        40        50
Pf Rd     AKWVCKICG YIYDEDAGDP DNGISPGTKF EELPDDWVCP ICGAPKSEFE KLED
Cp Rd     MKKYTCTVCG YIYNPEDGDP DNGVNPGTDF KDIPDDWVP  LGVGKDQFE EVEE
```

Rd from the mesophile, *Clostridium pasteurianum*, has been cloned and overexpressed in both iron- and zinc-containing forms (Eidsness et al., 1992; Mathieu et al., 1992). We report here the complete ^{1}H NMR assignments for wild-type zinc-containing Cp Rd (Cp ZnRd) and for a mutated Cp ZnRd (M1(−)K2AP15E Cp ZnRd) in which residues near the N-terminus, namely Met 1, Lys 2, and Pro 15, have been mutated to their counterparts, (−), Ala, and Glu, respectively, in Pf Rd. These residues, which are highlighted in Scheme 1, were among those proposed to contribute to thermostabilization of the β-sheet in Pf Rd (Blake et al., 1992). We address this proposed contribution by correlating NOE connectivities among residues within the β-sheet to thermostabilities of wild-type versus mutated Cp Rd.

Results

Recombinant protein characterization

Q-Sepharose chromatography completely resolved the apo-, Fe^{3+}, and Zn^{2+} forms of both recombinant wild-type and M1(−)K2AP15E Cp Rds (Eidsness et al., 1992). UV/vis absorption spectra of the Cp Fe^{3+}- and ZnRds are shown in Figure 1. The absorbance ratio A_{280}/A_{490} was found to be 2.36 and 2.39 for the wild-type and mutated recombinant Cp Fe^{3+}Rds, respectively, which are essentially identical to the published absorbance ratio, 2.4, for Cp Fe^{3+}Rd isolated originally from *C. pasteurianum* (Lovenberg & Walker, 1978). The absorption and EPR spectra (the latter not shown) for wild-type and mutated Cp Fe^{3+}Rds are essentially identical to each other, demonstrating that the $Fe^{3+}(SCys)_4$ site is not detectably affected by the mutations. ICP-AE analyses confirmed that the proteins identified as ZnRds in this study contained 1.0 mol Zn/mol Rd and no detectable iron. Amino acid analyses and N-terminal amino acid sequencing confirmed that the recombinant wild-type Cp ZnRd has an unblocked N-terminal Met residue, and that the M1(−)K2AP15E Cp ZnRd has an N-terminal Ala residue. These N-terminii are consistent with previous results on posttranslational processing of N-terminal Met residues in *Escherichia coli* (Hirel et al., 1989). The half-life of the visible absorption spectrum at 87 °C in 50 mM HEPES, pH 7.8, is approximately 3 h for both recombinant Cp wild-type and M1(−)K2AP15E Fe^{3+}Rds, whereas this half-life under the same conditions, is ≥90 h for Pf Rd (cf. Supplementary material in Electronic Appendix). These comparative results show that the M1(−)K2AP15E mutation does not significantly increase the thermostability of Cp Rd toward that of Pf Rd.

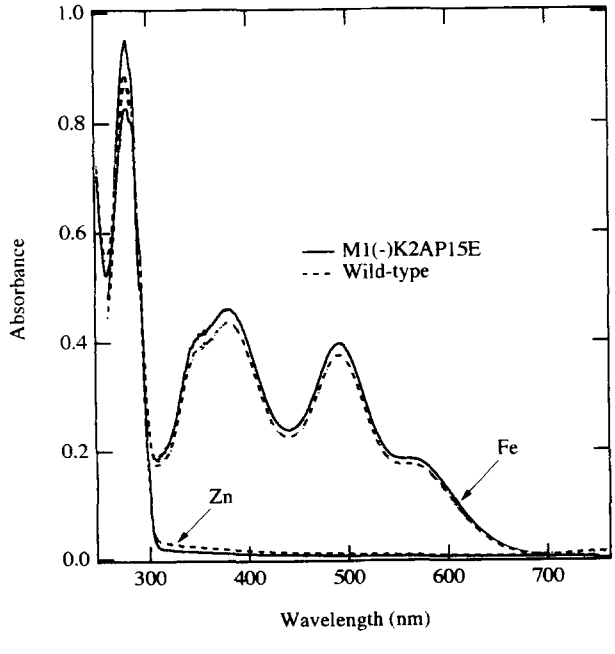

Fig. 1. UV/vis absorption spectra of recombinant wild-type and and M1(−)K2AP15E Cp Fe^{3+}- and ZnRds. Proteins were ~40 μM Fe^{3+}Rd and ~90 μM ZnRd in 50 mM HEPES, pH 8.2.

NMR assignments for recombinant Cp ZnRds

Assignments of the ^{1}H NMR signals were accomplished using standard methods (Wüthrich, 1986; Marion et al., 1989a). The spin systems of the various amino acid residues in the Rds were categorized and identified by their characteristic patterns of chemical shifts in 2D DQF-COSY, TOCSY, and 3D ^{1}H-^{15}N TOCSY-HSQC spectra. The coupling patterns of spin systems were examined with both 2D TOCSY and 3D ^{1}H-^{15}N TOCSY-HSQC spectra, and primary connectivities were established by DQF-COSY.

Wild-type Cp ZnRd spin system identification

Cp Rd contains 54 amino acid residues (Fig. 2), which can be classified as follows: 19 residues that normally have unique chemical shift patterns in the TOCSY fingerprint and side-chain regions (six Gly, five Val, three Thr, and five Pro), 21 residues whose $C_\alpha H$ is part of an AMX spin system (three Asn, eight Asp, four Cys, two Phe, one Trp, and three Tyr), and 14 residues with longer side chains (one Gln, five Glu, four Lys, one Met, two Ile, and one Leu). 2D ^{1}H-^{15}N HSQC (Fig. 3) revealed 49 peptide NH signals from a total of 59 NH cross peaks. These signals were correlated with those in the fingerprint region of the TOCSY spectrum (Fig. 4) and with those in the other spectra as described below.

Seventeen of the 19 spin systems with unique chemical shift patterns were identified readily: all six Gly, two of three Thr, all five Val, and four of five Pro. The upfield region of the 2D TOCSY and NOESY spectra clearly located four Pro spin systems. The amide region of the 3D ^{1}H-^{15}N TOCSY-HSQC spectrum revealed four NH_2 groups, three of which are identified readily as Asn by the characteristic NOESY cross peaks between NH_2 and C_βHs. The aromatic spin systems were assigned by the NOESY cross peaks between aromatic protons and C_βHs of AMX systems. One Phe spin system, later identified as Phe 30, exhibits two sets of aromatic protons in the TOCSY spectrum at 25 °C and 35 °C, but predominantly one set at 15 °C. We interpret these observations as indicating two distinct conformations or orientations of Phe 30 at the higher temperatures and only one predominant conformation/orientation at 15 °C. Phe 30

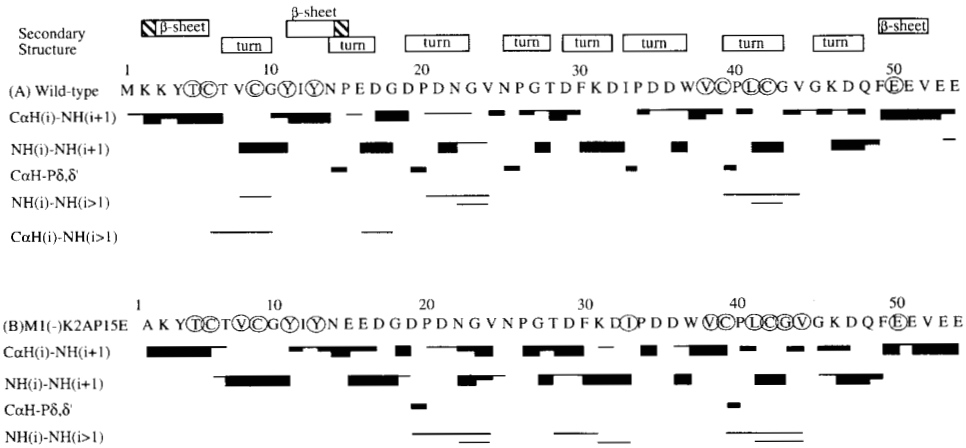

Fig. 2. Summary of secondary structure (white bars), NOE connectivities (black bars), and residues exhibiting slow peptide NH exchange rates (circled) for **(A)** wild-type and **(B)** M1(−)K2AP15E Cp ZnRds deduced from the NMR data. Relative NOE cross peak intensities are indicated by increasingly thick bars for weak, medium, and strong. NH(i)-NH($i > 1$) NOEs are between beginning and ending residues only. Cross hatches in the secondary structure bars indicate extensions of the β-sheet in the mutated Rd.

also apparently exhibits two chemical shift values in the ^{1}H-^{15}N 2D HSQC spectrum (one of which is labeled with a question mark in Fig. 3), but exhibits only one $C_{\alpha}H$-NH cross peak in 2D TOCSY and 3D TOCSY-HSQC spectra. Thirteen of 14 long side-chain spin systems are readily located: Gln 48 by its characteristic NOEs from the amide-NH_2 to $C_{\gamma}H_2$, both Ile (12 and 33) and Leu 41 by their characteristic side-chain chemical shift patterns in TOCSY and DQF-COSY, and three of four Lys residues. The remaining six spin systems arise from five Glu and one Lys residue.

Sequence-specific assignments for wild-type Cp ZnRd

The assigned spin systems are labeled in the 2D ^{1}H-^{15}N HSQC spectrum (Fig. 3) and the fingerprint region of the 2D TOCSY spectrum (Fig. 4). ^{1}H and ^{15}N chemical shifts for all residues

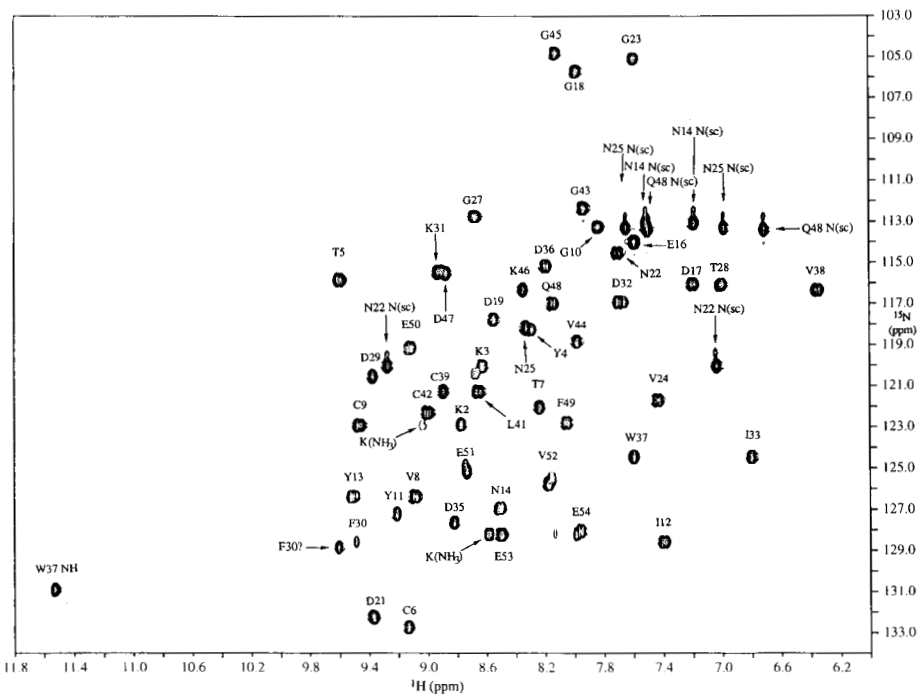

Fig. 3. 2D ^{1}H-^{15}N HSQC spectrum of uniformly ^{15}N-labeled wild-type Cp ZnRd observed at 25 °C. Assigned ^{1}H-^{15}N cross peaks for peptide and side-chain (sc) NHs are labeled by residue letter and number.

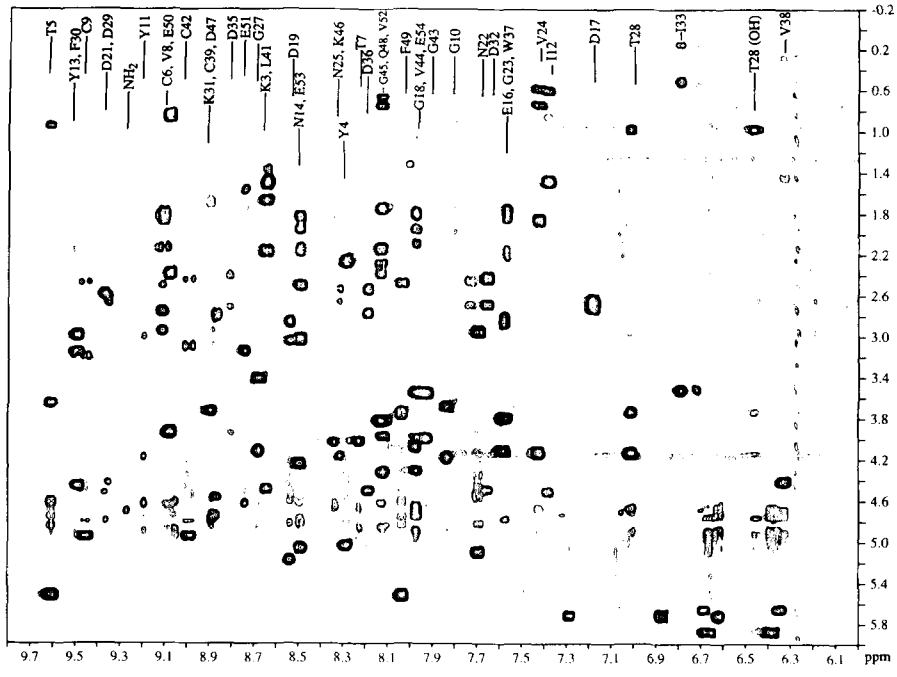

Fig. 4. Fingerprint region of the 25 °C TOCSY spectrum (60-ms mixing time) of wild-type Cp ZnRd. Assigned spin systems, which were detected via their NH resonance frequencies, are labeled by residue letter and number. The Met 1 spin system, detected via its $C_\alpha H$ frequency, is also labeled.

of wild-type Cp ZnRd are listed in Table 1. The assignments were initiated at the various unique residues identified in the preceding section: Gln 48, Trp 37, L41, and at Ile, Thr, Asn, Gly, and Val. The backbone NOESY connectivities, $C_\alpha H(i)$-$NH(i+1)$ and $NH(i)$-$NH(i+1)$ in 2D NOESY and 3D ^{15}N separated NOESY spectra were used for the assignments. For Pro residues, the sequential connectivity, $C_\alpha H(i)$-$C_{\delta,\delta'}H(i+1)$, in 2D NOESY spectra was used. The identified NOESY connectivities are summarized in Figure 2. The N-terminal segment, Met 1-Asn 14, was assigned based on the standard $C_\alpha H(i)$-$NH(i+1)$ NOESY cross peak pattern for Met 1-Thr 7, $NH(i)$-$NH(i+1)$ from Thr 7 to Tyr 11 and $C_\alpha H(i)$-$NH(i+1)$ from Gly 10 to Asn 14. The sequence Thr-Cys-Thr-Val (residues 5-8) is unique in Cp Rd (cf. Scheme 1). Therefore, the chemical shift patterns and connectivities expected for this fragment, particularly the AMX correlation pattern expected for the Cys residue between two Thr residues, were used as a starting point for establishing connectivities in the Met 1-Asn 14 segment. The $C_\alpha H$ and $C_\gamma H_3$ of Thr 7, which were absent in the fingerprint region of the 2D TOCSY spectrum, were observed in the 3D ^1H-^{15}N TOCSY-HSQC spectrum and in the upfield region of the 2D TOCSY spectrum. Although the N-terminal residue Met 1-NHs were not observed in the fingerprint region of the TOCSY spectra, the $C_\alpha H(1)$-NH(2) NOE connectivity observed in 2D NOESY at 15 °C identifies the chemical shift of Met 1-$C_\alpha H$. $C_\beta Hs$ of Met 1 were in turn identified through the $C_\alpha H$ resonance in 2D TOCSY. The intrastrand and interstrand NOEs were distinguished by the scalar connectivity patterns of the spin systems and the overall NOE pattern. For example, $C_\alpha H$ of Thr 5 has NOEs with two NH protons from two AMX spin systems, of which the Tyr 13 spin system was assigned by the NOEs between its $C_\beta Hs$ and aromatic protons. The other AMX spin system was assigned as Cys 6. As discussed below, several residues of the Met 1-Asn 14 segment also show NOE connectivities to other remote residues. The sequential connectivity of Asn 14 to Pro 15 was established by their $C_\alpha H$-$C_{\delta,\delta'}H$ NOE.

Other segments assigned through sequential backbone NOE connectivities include Pro 15-Asn 25, Pro 26-Asp 35, and Asp 36-Glu 54. The assignment for Pro 15-Asn 25 was initiated with the Asn residues. The segment was interrupted by the absence of a detectable NOE between Asn 25-$C_\alpha H$ and Pro 26-$C_{\delta,\delta'}H$. Starting from a Gly$C_\alpha H$-ThrNH NOE pattern, the assignment was extended from Pro 26 to Asp 35 by the backbone NOE connectivities. In the assignment of segment Asp 36-Glu 54, several residues were used to initiate the assignment, including Leu 41, two Gly, two Val, and Phe. No backbone NOE was observed between Asp 35 and Asp 36 in 2D NOESY recorded at 25 °C because the chemical shift of Asp 35-$C_\alpha H$ is very close to the solvent resonance. The $C_\alpha H(35)$-NH(36) NOE, however, is visible in 2D NOESY recorded at 15 °C. From Phe 49, strong- or medium-intensity $C_\alpha H(i)$-$NH(i+1)$ NOE connectivities extended the assigned segment to the N-terminal residue, Glu 54. These Phe 49-Glu 54 connectivities are shown in Figure 5.

Secondary structure of wild-type Cp ZnRd

The secondary structural elements identified in this work are shown schematically in Figure 2. Three extended segments were identified through strong $C_\alpha H(i)$-$NH(i+1)$ cross peaks in the 2D NOESY and 3D NOESY-HSQC spectra as participating in an antiparallel β-sheet. Strong interstrand NOEs indicate that the β-sheet involves 12 residues from three strands, Lys 3-Cys 6 (N-terminal), Tyr 11-Asn 14 (middle), and Phe 49-Val 52 (C-terminal). These NOE connectivities, shown schematically in

Table 1. *^1H and ^{15}N NMR chemical shifts of C. pasteurianum ZnRd at 25 °C*[a]

Residue	NH	Hα	Hβ	Other H	^{15}N[b]
1 Met	–	3.92[c]	2.37		
2 Lys	8.77	4.36	2.15	2.95, 2.02, 1.94, 1.82	123.93
3 Lys	8.66	4.83	1.68	2.81, 1.57, 1.50, 1.37	120.12
4 Tyr	8.29	5.04	2.28	H2,6 6.66; H3,5 6.46	118.24
5 Thr	9.62	5.52	3.66	γCH_3 0.95	115.78
6 Cys	9.11	2.95	2.76, 2.50		132.77
7 Thr	8.23	4.02		γCH_3 1.26	122.11
8 Val	9.08	3.94	2.39	γCH_3 0.91, 0.82	126.45
9 Cys	9.45	4.95	3.19, 2.50		123.05
10 Gly	7.80	4.20, 3.70			113.20
11 Tyr	9.19	4.19	3.19, 3.00	H2,6 7.33; H3,5 7.09	127.03
12 Ile	7.38	4.52	1.49	γCH_2 0.86; δCH_3 0.72; γCH_3 0.60	128.67
13 Tyr	9.48	4.46	3.18, 3.00	H2,6 7.16; H3,5 6.37	126.45
14 Asn	8.50	5.06	3.03, 2.51		127.03 (113.09)
15 Pro		5.12	2.54, 1.91	δCH_2 3.94, 3.87; 2.12	
16 Glu	7.57	3.80	2.19, 1.80	γCH_3 1.77	114.02
17 Asp	7.19	4.62	2.72, 2.65		106.02
18 Gly	7.97	4.00, 3.55			105.70
19 Asp	8.54	5.19	3.05, 2.87		117.37
20 Pro		4.11	2.30	δCH_2 3.92, 3.84; 2.10	
21 Asp	9.35	4.43	2.67		132.30
22 Asn	7.69	5.20	4.82		114.61 (120.00)
23 Gly	7.58	4.12, 3.80			105.00
24 Val	7.44	4.13	1.87	γCH_3 0.74, 0.59	121.76
25 Asn	8.31	4.17	2.66, 2.54		118.13 (113.32)
26 Pro		3.70	2.23, 1.21	δCH_2 3.40, 2.93; 1.79, 1.58	
27 Gly	8.68	4.12, 3.41			112.73
28 Thr	7.01	4.14	3.74	OH 6.47; γCH_3 0.98	116.13
29 Asp	9.37	4.53	2.60		120.59
30 Phe	9.50	3.16	2.19	H2,6[d] 5.81; 5.65[c]; H3,5[d] 6.38, 6.35[c]; H4[d] 6.68, 6.67[c]	128.55, 128.91?
31 Lys	8.89	3.73	1.65	2.95, 1.43, 1.37, 1.27	115.43
32 Asp	7.66	4.50	2.69, 2.42		116.84
33 Ile	6.79	3.53	0.93	γCH_2 0.51, 0.15; γCH_3 −0.01; δCH_3 −1.29	124.57
34 Pro		4.13	2.34, 1.90	δCH_2 3.22, 2.70; 2.01	
35 Asp	8.78	4.63	2.72, 2.41		127.62
36 Asp	8.19	4.50	2.77, 2.54		115.20
37 Trp	7.59	4.12	2.89, 2.83	H2 7.06; NH 11.52; H4 7.29; H5 6.87; H6 5.72; H7 6.62	124.45 (130.90)
38 Val	6.32	4.42	1.42	γCH_3 0.51, 0.28	116.37
39 Cys	8.89	4.79	3.10, 2.95		121.29
40 Pro		3.98	2.41, 1.72	δCH_2 3.74, 3.58; 2.01, 1.98	
41 Leu	8.65	4.41	2.17	γCH 1.65, 1.51, 1.05, δCH_3 0.79	121.29
42 Cys	9.01	4.95	3.11, 2.45		122.34
43 Gly	7.84	4.19, 3.86			112.38
44 Val	7.97	4.13	1.87	γCH_3 0.74, 0.60	118.83
45 Gly	8.12	4.32, 3.97			104.71
46 Lys	8.34	4.04	1.81	2.63, 1.58, 1.19	116.37
47 Asp	8.87	4.57	2.80		115.55
48 Gln	8.14	4.86	2.39, 2.28	2.15	116.95 (113.44)
49 Phe	8.04	5.52	3.76, 2.48	H2,6 7.27; H3,5 7.49; H4 7.59	122.81
50 Glu	9.12	4.84	2.14	1.83, 1.80	119.18
51 Glu	8.74	3.15	1.75	1.57	125.16
52 Val	8.14	3.83	1.75	γCH_3 0.76, 0.67	125.86
53 Glu	8.49	4.25	2.16, 2.14	1.95, 1.84	128.21
54 Glu	7.97	4.08	2.10, 1.95	1.81	128.20

[a] $\delta \pm 0.01$ ppm relative to DSS for ^1H.
[b] Peptide (side chain) $\delta \pm 0.05$ ppm relative to liquid NH_3.
[c] At 15 °C.
[d] Both shifts observed at 25 °C.

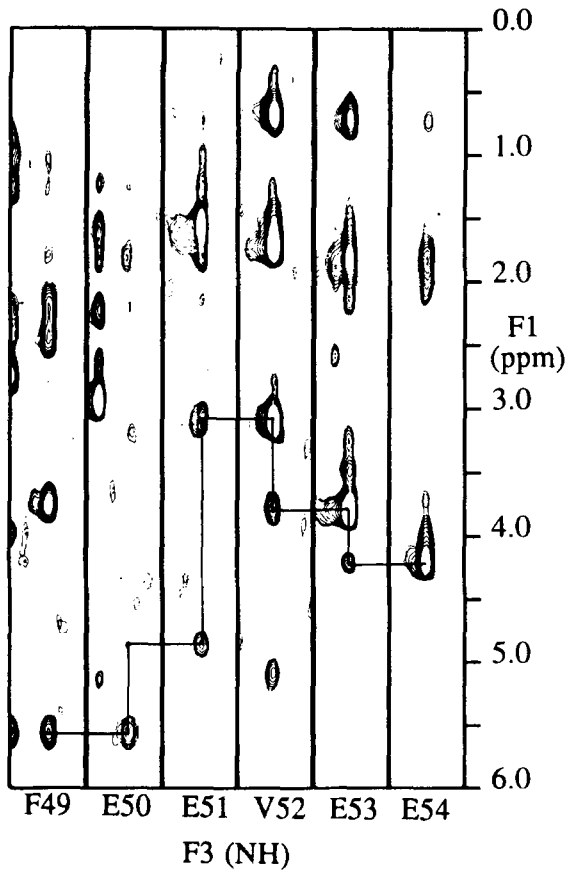

Fig. 5. 2D strips from a 3D ^{1}H-^{15}N NOESY-HSQC spectrum of uniformly ^{15}N-labeled wild-type Cp ZnRd showing sequential $C_\alpha H(i)$-NH(i + 1) NOE connectivities for residues Phe 49–Glu 54. The spectrum was obtained at 25 °C with a mixing time of 150 ms.

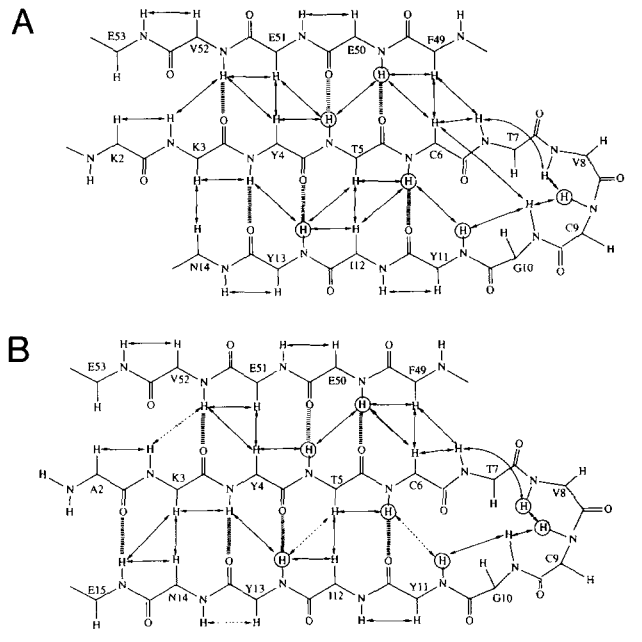

Fig. 6. Schematic representation of the triple-stranded β-sheet and the turn connecting the N-terminal and middle strands for **(A)** wild-type Cp ZnRd and **(B)** M1(−)K2AP15E Cp ZnRd. Double-headed arrows indicate observed NOEs that were used in determining residues in the β-sheet. Dotted double-headed arrows indicate NOEs not observed due to degeneracy of the cross peaks. Inferred interstrand hydrogen bonds are shown by dashed lines. Slowly exchanging NH protons are circled.

Figure 6, indicate the presence of three hydrogen bonds between the N- and C-terminal strands (two between residues 5 and 50, and one between residues 3 and 52), and an additional three between the middle and N-terminal strands (two between residues 4 and 13 and one between residues 6 and 11). Although the C-terminal $C_\alpha H(i)$-NH(i + 1) NOE connectivity extends to Glu 54, the absence of detectable interstrand $C_\alpha H$-$C_\alpha H$ NOEs between Lys 2 and Glu 53 at all three temperatures indicates that no hydrogen bond is formed by the carbonyl oxygen of Met 1 with the amide proton of Glu 54. We failed to observe a Q48$C_\alpha H$-F49NH NOE, which would be needed for inclusion of residue 48 in the β-sheet.

Several segments are identified to form tight turns by the strong characteristic NH(i)-NH(i + 1) NOEs. The absence of $C_\alpha H(i)$-NH(i + 3) NOEs indicates no helical structure in any of these segments. Immediately following the N-terminal strand of the β-sheet, residues Thr 7–Gly 10 form a well-defined Type I turn (Baker & Hubbard, 1984), indicated by strong sequential NH(i)-N(i + 1) NOEs (shown schematically in Fig. 6). This turn is characterized by hydrogen bonding of the Thr 7 carbonyl group to the Gly 10 peptide N-H. The side-chain hydroxyl group of Thr 7 also likely participates in a hydrogen bond to the peptide N-H of Cys 9 to form an Asx turn (Rees et al., 1983; Kissinger et al., 1991). This turn connects the N-terminal and middle strands of the β-sheet.

Additional turns were identified by their well-defined, sequential NH(i)-N(i + 1) NOEs. Four type I/Asx turns were identified with Asp or Asn being the initiators of the turns: Asn 14–Gly 18, Asp 19–Gly 23, Asp 25–Thr 28, and Asp 29–Asp 32. These turns are defined by medium to strong sequential NH(i)-NH(i + 1) NOEs of Glu 16–Gly 18, Asp 21–Asn 22, Gly 27–Thr 28, and Phe 30–Asp 32, respectively. Residues Cys 39–Gly 43 also form a Type I/Asx turn defined by the NH(41)-NH(42) and NH(42)-NH(43) NOEs, which differs from the other Type I/Asx turns by the likely involvement of Cys 39 S_δ in a hydrogen bond with Leu 41 amide group. Two Type I turns are formed by residues Ile 33–Trp 37 and Gly 45–Gln 48; these turns were identified by the strong continuous NH(i)-N(i + 1) NOEs of Asp 36–Trp 37 and Lys 46–Gln 48, respectively. Based on our NMR data, seven residues in Cp ZnRd participate in neither turns nor β-sheet: the two N-terminal residues, the two C-terminal residues, and Val 24, 38, and 44. Val 24 is likely involved in two hydrogen bonds: the Val 24 carbonyl group with the Asp 19 amide group and the Val 24 amide group with the Asp 19 carbonyl group. These bonds are manifested by the NH(19)-NH(24) and $C_\alpha H$(20)-NH(24) NOEs.

Slowly exchanging peptide NHs in wild-type Cp ZnRd

Eleven slowly exchanging peptide NH protons were observed in the 2D NOESY and TOCSY spectra of Cp ZnRd. These spectra were recorded at 25 °C within 20 h of exchanging the sample into D_2O and storage at 4 °C. Six of these slowly exchanging NH protons, those of Thr 5, Cys 6, Cys 9, Tyr 11, Tyr 13, and Glu 50, were assigned to residues either within the β-sheet or to

the turn connecting the first two strands of the β-sheet, as shown in Figure 5. The remaining five slowly exchanging peptide NHs were assigned to Val 38, Cys 39, Leu 41, Cys 42, and Val 44. With the exception of Val 38, these latter residues occur in turn regions of secondary structure, as identified in this study. Residues with slowly exchanging peptide NHs, as defined in this work, are circled in Figure 2.

M1(−)K2AP15E Cp ZnRd spin system identification

Spin systems for the mutated Cp ZnRd were identified by comparing the patterns of scalar correlations in the 2D TOCSY spectrum and NOEs in the 2D NOESY spectrum recorded at 25 °C for the mutant sample with the 2D spectra recorded for the wild-type protein under the same conditions. Although the chemical shift of Ala 2 NH_2 (Ala 2 being the N-terminal residue in this mutant, cf. Fig. 2B) was not observed, Ala 2-$C_\alpha H$ was identified by the strong $C_\alpha H(2)$-NH(3) NOE cross peak in the 2D NOESY spectrum. The ^1H chemical shifts for all residues of Cp M1(−)K2AP15E ZnRd are listed in Table 2.

Comparisons of the M1(−)K2AP15E Cp ZnRd NMR data to that of wild-type Cp ZnRd

A plot of the peptide NH ^1H chemical shift perturbations in the mutated versus wild-type ZnRd is shown in Figure 7. The largest such perturbation (≈1 ppm) occurs for the peptide NH of Tyr 4, and the peptide NHs of Gly 27 and Phe 30 also show chemical shift perturbations of ≥0.5 ppm. The aromatic NH of Trp 37 is shifted 1.20 ppm upfield in the mutated relative to the wild-type Cp ZnRd. In contrast to the wild-type, Phe 30 in M1(−)K2AP15E Cp ZnRd shows only a single set of aromatic resonances in the TOCSY spectrum at all three temperatures (15, 25, and 35 °C).

The NMR data for the mutated Cp ZnRd define a triple-strand β-sheet analogous to that observed in the wild-type Cp ZnRd. The NOEs that define this β-sheet in the mutated Rd are shown schematically in Figure 6B. The NOEs for the mutated ZnRd also indicate that the residues involved in turn regions are the same as those for wild-type ZnRd, when the sequences are aligned as in Figure 2. Two important differences from the wild-type ZnRd are noted. A hydrogen bond between the carbonyl of the N-terminal residue, Ala 2, and the amide of Glu 15 is indicated by the strong $C_\alpha H(3)$-$C_\alpha H(14)$, $C_\alpha H(3)$-NH(3), and medium $C_\alpha H(3)$-NH(15) NOEs. The absence of NH(3)-NH(52) and $C_\alpha H(2)$-$C_\alpha H(53)$ NOEs indicates no hydrogen bond formed between the Lys 3 amide group and the Val 52 carbonyl group. The second important difference is the more intense NOE cross peaks in the spectrum of the mutated Rd versus wild-type Rd, as illustrated by comparison of the normalized NOESY spectra in Figure 8.

The most upfield signal in the ^1H NMR spectrum of the wild-type Cp ZnRd has been assigned to the δ-methyl group of Ile 33. This signal is shifted 0.14 ppm downfield for the mutated Cp ZnRd. The δ-methyl group of Ile 33 has several NOEs to other protons, which appear in the NOESY spectra of both wild-type and mutated proteins. As shown in Figure 9, the normalized NOE cross peak intensities of Ile 33 are stronger for the mutated than wild-type Cp ZnRd.

Residues identified as having slowly exchanging peptide NHs in the D_2O-exchanged sample of the mutated ZnRd are circled in Figure 2. The mutated Rd exhibits three slowly exchanging peptide NHs in addition to those observed in the wild-type Rd, namely, those of Val 8, Ile 33, Gly 43. All of these additional slowly exchanging peptide NHs lie in turn regions, as identified by our NMR data.

Discussion

Comparison of Cp ZnRd structure deduced from NMR data versus Cp FeRd X-ray crystal structure

Our NMR data have identified 48 of 54 residues in the recombinant wild-type Cp ZnRd as participating in specific kinds of secondary structural elements. From the X-ray crystal structure of Cp Fe^{3+}Rd (Watenpaugh et al., 1979; Sieker et al., 1994), a three-stranded, antiparallel β-sheet consisting of residues 3–7, 11–13, and 48–52 was identified, based on backbone conformation. These ranges are close to those found for Cp ZnRd in the present NMR study based on NOE connectivities: 3–6, 11–14, and 49–52. Except for that between the Q48 carbonyl and K7 peptide NH, the backbone hydrogen bonding pattern in this β-sheet inferred from the observed interstrand NOEs is identical to that observed in the crystal structure (Watenpaugh et al., 1979). Eight well-defined Type I (Baker & Hubbard, 1984) or Type I/Asx turns (Rees et al., 1983) were identified by NOE connectivities, and the regions defining these turns (Fig. 2) are essentially identical to those observed in the X-ray crystal structure. One turn connects the N-terminal and middle strands of the β-sheet (Fig. 6), and the remaining seven turns are located between the end of the middle strand of the β-sheet (Asn 14) and the beginning of the C-terminal strand of the β-sheet (Phe 49). The 11 peptide NHs of wild-type Cp ZnRd that we classify as slowly exchanging with solvent (circled in Fig. 2) include those of the only four Cys residues, 6, 9, 39, and 42. These residues are known to provide the metal ligands to the $M(SCys)_4$ site. The X-ray crystal structure of Cp FeRd shows that the peptide NHs of Cys 9, Tyr 11, Leu 41, Cys 42, Val 8, and Val 44 are in position to form N-H–S hydrogen bonds involving the four Cys residues (Watenpaugh et al., 1979). Of these NHs, all but that of Val 8 were identified as slowly exchanging NHs in the wild-type Cp ZnRd, and the Val 8 NH was added to the slowly exchanging group in the mutated Cp ZnRd.

Comparisons of NMR and structural data among wild-type Cp ZnRd, M1(−)K2AP15E Cp Zn Rd, and Pf ZnRd

Significant NH ^1H chemical shift perturbations occur in mutated versus wild-type Cp ZnRd for residues that are sequentially both proximal (e.g., Tyr 4, Asn 14, and Glu 16) and distal (e.g., Gly 27, Phe 30, Val 52, and Trp 37 aromatic NH) to the mutation positions, 2 and 15, in the sequence (cf. Fig. 7 and Tables 1, 2). Only one ^1H of the metal-binding Cys residues, a Cys 39 Hβ, shows a significant chemical shift perturbation in the mutated ZnRd, consistent with the lack of any detectable spectroscopic perturbation of the FeS_4 site in the mutated Fe^{3+}Rd.

The secondary structure of both wild-type and mutated Cp ZnRds, as determined by NMR methods, includes one triple-stranded β-sheet and eight turns. The beginning and ending residues for the turns are essentially the same in the wild-type and mutated Cp ZnRds, when the sequences are aligned as shown

Table 2. *^{1}H NMR chemical shifts of C. pasteurianum M1(−)K2AP15E-ZnRd at 25 °C*[a]

Residue	NH	Hα	Hβ	Others
2 Ala	–	4.13	1.57	
3 Lys	8.74	5.46	1.57, 1.48	2.87, 1.40, 1.21
4 Tyr	9.31	4.95	2.59, 2.39	H2,6 6.61; H3,5 6.45
5 Thr	9.47	5.55	3.70	γCH_3 1.01
6 Cys	9.21	3.05	2.86, 2.55	
7 Thr	8.27	4.54	4.05	γCH_3 1.20
8 Val	9.08	3.99	2.43	γCH_3 0.91, 0.89
9 Cys	9.47	4.99	3.23, 2.51	
10 Gly	7.94	4.23, 3.71		
11 Tyr	9.21	4.22	2.99, 3.20	H2,6 7.35; H3,5
12 Ile	7.29	4.72	1.53	γCH_2 0.96, 0.94, δCH_3 0.78, γCH_3 0.65
13 Tyr	9.47	4.63	3.31, 3.08	H2,6 7.15; H3,5 6.37
14 Asn	8.80	4.84	3.02, 2.51	
15 Glu	8.51	3.85	2.20	1.88
16 Glu	7.85	3.84	2.25	1.85
17 Asp	7.01	4.71	2.80, 2.66	
18 Gly	7.93	4.05, 3.62		
19 Asp	8.53	5.21	3.06, 2.94	
20 Pro		4.12	2.26	4.03, 3.87, 2.15
21 Asp	9.32	4.47	2.72	
22 Asn	7.75	5.15	3.05, 2.94	
23 Gly	7.67	4.68, 3.85		
24 Val	7.50	4.18	1.89	γCH_3 0.80, 0.61
25 Asn	8.39	4.23	2.70, 2.58	
26 Pro		3.70	2.27, 1.40	3.46, 1.83, 1.63
27 Gly	8.07	3.85, 3.62		
28 Thr	7.14	4.09	3.84	OH 6.52, γCH_3 1.01
29 Asp	9.16	4.38	2.66, 2.54	
30 Phe	10.22	3.37	2.55, 2.19	H2,6 6.15; H3,5 6.49; H4 6.76
31 Lys	8.80	3.82	1.77	2.96, 1.69, 1.35
32 Asp	7.64	4.52	2.49	
33 Ile	6.84	5.76	3.52	γCH_2 0.57, 0.15; γCH_3 0.02; δCH_3 −1.14
34 Pro		4.17	2.43	3.80, 3.31, 2.12, 1.99
35 Asp	8.82	4.81	2.77, 2.46	
36 Asp	8.21	4.52	2.71, 2.50	
37 Trp	7.67	4.16	2.92	H2 7.11; NH 11.25; H4 7.31 H5 6.83; H6 5.75; H7 6.65
38 Val	6.30	4.43	1.50	γCH_3 0.36
39 Cys	8.92	4.77	3.82, 3.04	
40 Pro		3.99	2.52, 1.83	3.74, 2.19, 2.10
41 Leu	8.64	4.53	2.15, 1.75	1.59, 1.11, 0.88
42 Cys	9.05	4.99	3.19, 2.50	
43 Gly	7.98	4.04, 3.61		
44 Val	8.00	4.34	2.31	γCH_3 1.16, 1.09
45 Gly	8.14	4.36, 4.00		
46 Lys	8.34	4.10		2.16, 2.04, 1.87
47 Asp	8.86	4.60	2.88, 2.80	
48 Gln	8.19	4.71	2.44, 2.35	2.23
49 Phe	8.05	5.56	3.82, 2.52	H2,6 7.34; H3,5 7.51; H4 7.62
50 Glu	9.03	4.85	2.23, 2.18	1.98, 1.83
51 Glu	8.88	3.49	1.87	1.67
52 Val	8.43	3.93	1.82	γCH_3 0.78
53 Glu	8.50	4.28	2.24, 2.15	2.04, 1.91
54 Glu	8.02	4.11	2.13	1.99, 1.84

[a] δ ± 0.01 ppm relative to DSS.

in Figure 2. However, our NMR data indicate an extension of the β-sheet in the M1(−)K2AP15E Cp ZnRd to include Ala 2 and Glu 15. The mutated Cp Rd also shows more intense NOEs (Fig. 8), indicating stronger interactions between the strands of the β-sheet, and, in fact, throughout the mutated Rd. Peptide NHs of three additional residues, Val 8, Ile 33, and Gly 43, were identified as slowly exchanging in the mutated Cp ZnRd. Ile 33, which lies within the hydrophobic core of Cp Rd (Watenpaugh

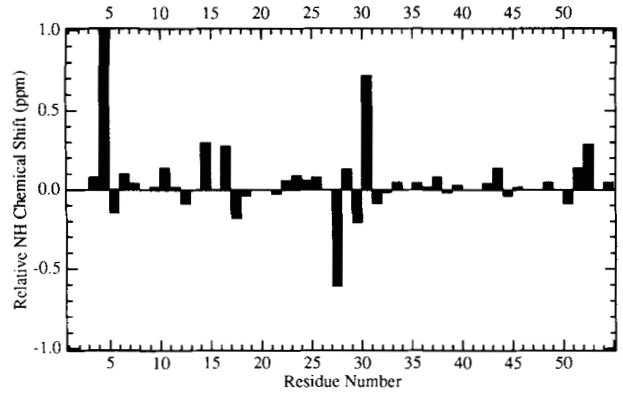

Fig. 7. Histogram of peptide NH ^{1}H NMR chemical shifts of M1(−)K2AP15E Cp ZnRd relative to those of wild-type Cp ZnRd.

et al., 1979), shows relatively stronger NOEs between its δ-methyl and surrounding protons in the mutated Cp ZnRd (cf. Fig. 9). The Phe 30 NH in the mutated Cp ZnRd shows additional NOE cross peaks to an Asp 29 $C_\beta H$ and a Cys 39 $C_\beta H$, which are not observed in spectra of the wild-type protein. These observations, together with the single set of aromatic resonances for Phe 30 versus two sets in the wild-type Cp ZnRd spectra, all indicate that the M1(−)K2AP15E Cp ZnRd has an overall tighter structure than does wild-type Cp ZnRd.

We have not detected any significant inconsistencies between our assignments for the two Cp ZnRds and those made previously for similar residues in Pf ZnRd (Blake et al., 1991). The NOEs and chemical shift patterns in the mutated Cp ZnRd are generally more reminiscent of those seen in Pf ZnRd (Blake et al., 1991). For example, they indicate formation of a hydrogen bond between the Ala 2 carbonyl and Glu 15 amide in both the mutated Cp and Pf ZnRds (Blake et al., 1991). In addition, only a single set of Phe 30 aromatic resonances is observed for both the mutated Cp and Pf ZnRds (Blake et al., 1991). Based on X-ray crystallography (Day et al., 1992), the Phe 30 NH in Pf Rd forms a hydrogen bond to a side-chain carboxylate oxygen of Glu 15. The analogous hydrogen bond could be the reason for our observation of only one set of Phe 30 aromatic resonances for the M1(−)K2AP15E Cp ZnRd versus two sets for wild-type Cp ZnRd, where the analogous hydrogen bond cannot form. Although we did not detect NOEs between the Phe 30

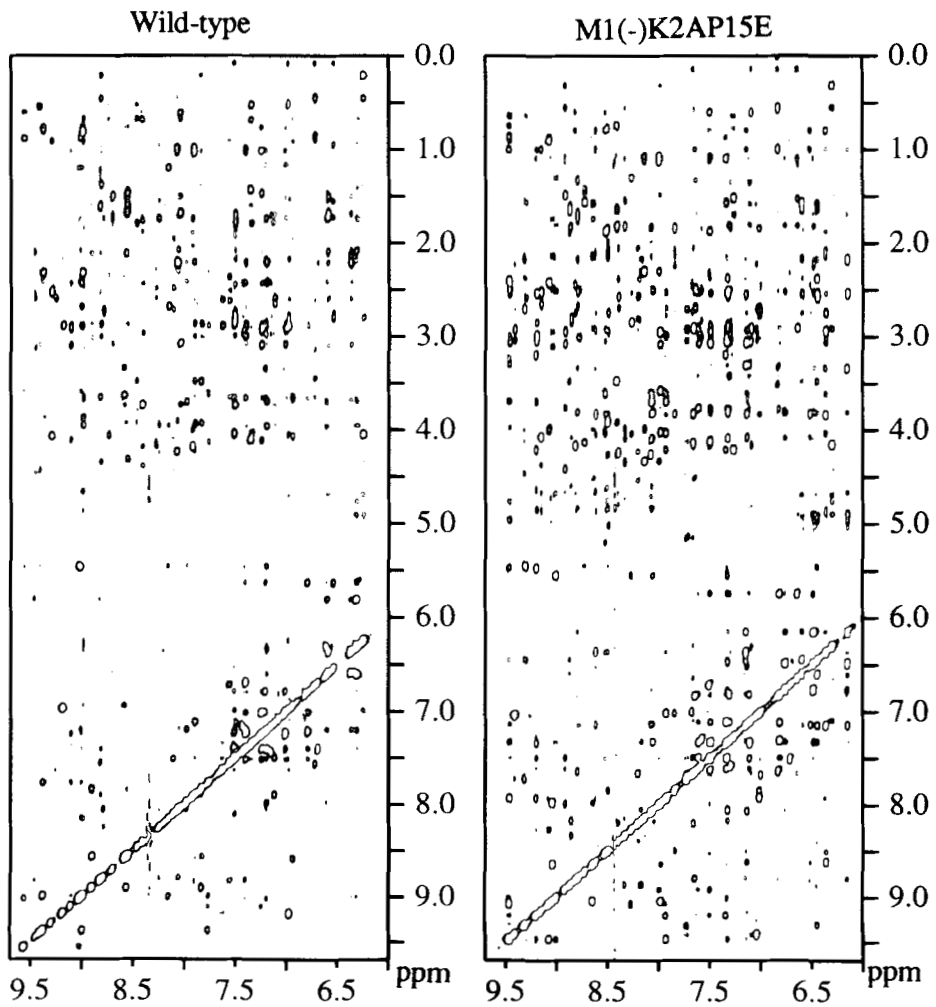

Fig. 8. 2D NOESY spectra observed at 25 °C with a mixing time of 300 ms for wild-type and M1(−)K2AP15E Cp ZnRds. Both spectra are plotted to the same contour level and normalized to equal intensities of aromatic cross peaks of Phe 49, Tyr 11, and Tyr 14.

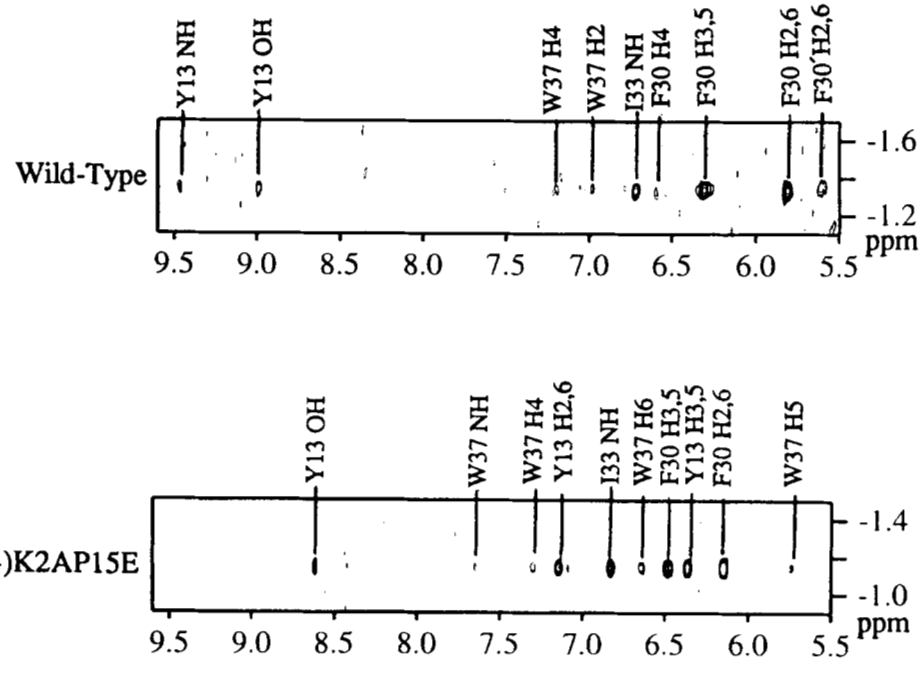

Fig. 9. Portions of the 2D NOESY spectra showing Ile 33 cross peaks for wild-type and mutated Cp ZnRd. Both spectra are plotted to the same contour level and normalized as described in the legend to Figure 8. Assigned cross peaks are labeled by residue letter and number.

NH and any Glu 15 proton in spectra of the M1(−)K2AP15E Cp ZnRd, neither were such NOEs reported for Pf ZnRd (Blake et al., 1991, 1992).

Secondary structure and thermostability of Rds

The interstrand interactions within the β-sheet of the mutated Cp Rd derived from our NMR study resemble those seen in Pf Rd (Blake et al. 1991, 1992; Day et al., 1992), particularly the extension of the β-sheet to include Ala 2 and Glu 15. This extension, plus the shortening of the N-terminus by one residue in the mutated Cp Rd, could facilitate favorable electrostatic interactions involving the N-terminal Ala 2 amino group with the side-chain carboxylates of Glu 52 and Glu 15, as proposed for Pf Rd (Blake et al., 1991). An additional hydrogen bond in Pf Rd, involving the indole NH of Trp 4 and the carboxylate of Glu 15 (cf. Scheme 1) was also proposed to contribute to thermostabilization of the β-sheet (Blake et al., 1992; Day et al., 1992). Although the corresponding residue, Tyr 4 in Cp Rd, was not mutated in the present study, Elkin (1995) showed that an M1(−)K2AY4WT5VT7KP15E mutated Cp Fe^{3+}Rd in which all but one of the residues in the first two strands of the β-sheet were changed to their counterparts in Pf Rd (cf. Scheme 1) had a visible absorption half-life at 87 °C of ~6 h compared to ~3 h for wild-type Cp Fe^{3+}Rd and ≥90 h for Pf Fe^{3+}Rd (cf. Supplementary material in Electronic Appendix). These results, together with those in the present NMR study, suggest strongly that *the key to the extraordinary thermostability of Pf Rd does not lie in a unique set of hydrogen bonds and electrostatic interactions that inhibit "unzipping" of the N-terminal strand of the β-sheet*. The NMR results also suggest that an overall tighter protein structure does not necessarily lead to increased thermostability. Further studies on "chimeric" Pf/Cp Rds are in progress in order to delineate which regions of the Pf Rd structure contribute to its extraordinary thermostability.

Materials and methods

Construction of plasmids containing Rd genes

Molecular biology procedures generally followed those described in Sambrook et al. (1989) or in Ausubel et al. (1990). Nucleotide sequences of all new plasmids constructed in this work were verified by DNA sequencing in the Molecular Genetics Instrumentation Facility at the University of Georgia. Oligonucleotides were purchased from Integrated DNA Technologies, Inc. Procedures for cloning, amplification, and other manipulations of the Cp Rd gene followed those described by Zeng et al. (1995). A synthetic gene coding for Cp Rd (Eidsness et al., 1992) was corrected to that coding for a more recently published wild-type amino acid sequence (Mathieu et al., 1992) and ligated into the *Nde* I/*Hin*d III restriction sites of plasmid pT7-7 (Tabor, 1990). The resulting plasmid, pNNQ, was transformed into *E. coli* strain BL21(DE3) (Novagen, Inc.) (Studier et al., 1990). The mutation, K2A,P15E, was introduced into the Rd gene of pNNQ by PCR, as described by Elkin (1995). The resulting plasmid, pCE-1, was transformed into *E. coli* strain BL21(DE3).

Overexpression, purification, and characterization of recombinant Rds

Freshly transformed *E. coli* BL21(DE3)[pNNQ] was cultured in 1-L batches of Luria-Bertani medium containing 100 μg/mL of ampicillin in an incubator/shaker at 37 °C until $OD_{600} \approx 1.0$,

at which point IPTG was added to a final concentration of 0.4 mM. The cultures were incubated with shaking for an additional 3 h at 37 °C and the cells were then harvested by centrifugation (5,000 × *g*, 4 °C) and stored at −80 °C if not used immediately.

The harvested cells were lysed by three −80 °C freeze/thaw cycles (Johnson & Hecht, 1994) and resuspended in 50 mM Tris-HCl, pH 7.4. After centrifugation (30,000 × *g* at 4 °C), the resulting supernatant was concentrated in an Amicon cell fitted with a YM-3 membrane to a volume of ~5.0 mL. The Rd was purified on a Q-Sepharose column (Pharmacia LKB) in 50 mM Tris-HCl, pH 7.4, with a linear gradient from 0.2–0.5 M NaCl, which separated the FeRd from ZnRd (Eidsness et al., 1992). The Cp M1(−)K2AP15E Fe- and ZnRds were overexpressed, isolated, and purified from *E. coli* BL21(DE3)[pCE1] using procedures identical to those described for Cp ZnRd. Yields were ~6 mg/L culture for FeRds and ~12 mg/L culture for ZnRds. Uniformly ^{15}N-enriched wild-type Cp ZnRd was obtained from cultures of freshly transformed *E. coli* BL21(DE3)[pNNQ] grown on M9 minimal medium supplemented with 0.4% glucose, 1.0 g/L of $^{15}NH_4Cl$ (Isotec Inc., 99.9% ^{15}N isotopic abundance), 0.1 mM $CaCl_2$ and 2 mM $MgSO_4$, and 100 μg/mL of ampicillin. One-liter cultures were grown at 37 °C to an $OD_{600} \approx 1.0$, at which point IPTG was added to 0.4 mM, followed by 25 mg of $ZnSO_4$. Further incubation of cultures, harvesting of cells, and protein purification and storage were conducted in a manner identical to that described above for the natural isotopic abundance Rd. Addition of the $ZnSO_4$ resulted in overexpression of essentially only the ZnRd. Yield of ^{15}N-labeled Cp ZnRd was ~5 mg/L culture. The purified Fe- and ZnRds were stored at −80 °C until used.

Inductively coupled plasma-atomic emission (ICP-AE) analyses of the metal contents in the Rds were performed in the Chemical Analysis Laboratory at the University of Georgia. Cp ZnRd protein concentrations were estimated using $\epsilon_{280} = 9{,}530$ M^{-1} cm^{-1} (Eidsness et al., 1992). UV/vis absorption spectra were obtained on a Shimadzu UV-2101PC spectrophotometer. N-terminal amino acid sequencing of ZnRds was performed at the Harvard Michrochemical Facility, Cambridge, MA.

NMR sample preparation

The purified Cp ZnRds were dialyzed against 100 mM phosphate and 150 mM sodium sulfate, pH 6.0, in an Amicon cell fitted with a YM-3 membrane. The samples were concentrated to approximately 4 mM Rd in 90% H_2O/10% D_2O containing 100 mM sodium phosphate and 150 mM sodium sulfate, pH 7.0. Uniformly ^{15}N-labeled Cp ZnRd sample was prepared in a manner identical to the natural isotopic abundance sample and was approximately 6 mM in Rd. Wild-type and mutated Cp ZnRd samples (4 mM) in D_2O were prepared from the phosphate-buffered H_2O samples by four cycles of lyophilization and redissolution in D_2O (100.0% D isotopic abundance, Aldrich Chemical Co.).

NMR spectroscopy

All spectra were acquired on a Bruker AMX400 spectrometer (400.1373 MHz, ^{1}H). ^{1}H chemical shifts were referenced to DDS, via the HDO resonance frequency at 4.86 ppm at 15 °C, 4.76 ppm at 25 °C and 4.66 ppm at 35 °C. ^{15}N chemical shifts were referenced to liquid NH_3 via ammonium chloride (Srinivasan & Lichter, 1977). 2D Phase-sensitive ^{1}H DQF-COSY (Rance et al., 1983), TOCSY (HOHAHA, Bax & Davis, 1985), and NOESY (Jeener et al., 1979) spectra were recorded at 15, 25, and 35 °C with a spectral width of 6,410 Hz for both dimensions. The water signal was suppressed by a Dante pulse train (Morris & Freeman, 1978) consisting of 5° pulses separated by 100-μs intervals, followed by a 40–60-ms SCUBA sequence (Brown et al., 1988) to allow for magnetization recovery of resonances close to the water frequency. A total of 2,048 complex data points were collected with 512 t_1 increments and 64 transients for each t_1 increment. Quadrature detection in the t_1 dimension was obtained using hypercomplex mode (States et al., 1982). For 2D TOCSY experiments, a spin lock field of 10.5 kHz was used during the DIPSI-2 (Shaka et al., 1988) mixing time of 60 ms, which includes 1-ms trim pulses. NOESY spectra were recorded with 150- and 300-ms mixing times. The 2D NOESY and TOCSY spectra of samples in D_2O were recorded at 25 °C within 20 h after exchanging the samples into D_2O and storage at 4 °C.

2D ^{1}H-^{15}N HSQC (Bodenhausen & Ruben, 1980; Bax et al., 1990) spectra were acquired at 25 and 35 °C for the uniformly ^{15}N-labeled Cp ZnRd with a spectral width of 6,410 Hz for the ^{1}H dimension and 2,433 Hz for the ^{15}N dimension. The spectrometer frequency in ^{1}H dimensions was set on the water resonance to achieve water suppression using the Dante pulse sequence followed by the SCUBA pulse sequence, as described above. 3D ^{1}H-^{15}N TOCSY-HSQC and 3D ^{1}H-^{15}N NOESY-HSQC (Fesik & Zuiderweg, 1988; Marion et al., 1989a, 1989c) spectra were recorded at 25 °C with spectral width of 6,410 Hz for the ^{1}H dimensions and 2,433 Hz for the ^{15}N dimension. For all ^{1}H-^{15}N experiments, quadrature detection in the indirectly observed dimensions was obtained using States-TPPI methods (Marion et al., 1989b) and initial increment delays were set so as to achieve the zero-order and first-order phase corrections of 90°, −180°, respectively (Bax et al., 1991). A total of 1,024 complex points were collected with 128 t_1 (^{1}H) and 40 t_2 (^{15}N) increments and 32 transients for each increment. For the TOCSY-HSQC experiment, a spin lock field of 10.5 kHz was used during the DIPSI-2 mixing time of 60 ms. The NOESY spectrum was recorded with a 150-ms mixing time.

All of the NMR data were processed and analyzed on a Silicon Graphics Indigo2 Workstation using NMRPipe, CAPP, and PIPP software (NIH). The 2D ^{1}H data were processed with 60°-shifted sine-bell-squared functions for NOESY and TOCSY spectra and with 5°-shifted sine-bell-squared functions for DQF-COSY spectra. The data sets were zero-filled to a final matrix size of 2,048 × 2,048 real points prior to Fourier transformation. The 2D ^{1}H-^{15}N HSQC were processed with 45°-shifted sine-bell-squared functions in both ^{1}H-^{15}N dimensions and zero-filled to 2,048 × 1,024 real data points prior to Fourier transformation. The left half of the data in ^{1}H dimension were extracted to yield a final matrix size of 1,024 × 1,024 real points. The 3D TOCSY-HSQC and NOESY-HSQC data were processed using a lowpass solvent filter prior to applying a 80°-shifted sine-bell-squared function and left-extracted after Fourier transformation in the t_3 dimension. An 80°-shifted sine-bell-squared function was applied in the t_1 (^{1}H) dimension, followed by zero-filling, Fourier transformation, and baseline correction. The t_2 (^{15}N) interferograms were processed with an 80°-shifted sine-bell-squared function, zero-filling, and Fourier transforma-

tion. The spectra had a final matrix size of 512 × 128 × 1,024 real data points.

Supplementary material in Electronic Appendix

Thermostability data at 87 °C in the form of fractional absorbance at 490 nm versus time for *C. pasteurianum* wild-type, M1(−)K2AP15E and M1(−)K2AY4WT5VT7KP15E Fe^{3+}rubredoxins, and *P. furiosus* wild-type Fe^{3+}rubredoxin are found in the Electronic Appendix.

Acknowledgments

This research was supported by National Institutes of Health grant GM50736 (D.M.K.) and by a National Science Foundation Research Training Group Award to the Center for Metalloenzyme Studies (DIR 90-14281). We thank Frank Delagio, Dan Garrett, and the Laboratory of Chemical Physics at NIH for providing the NMR software, and Sonia O'Dell for construction of plasmid pNNQ.

References

Adams MWW, Kelly RM. 1995. Enzymes from microorganisms in extreme environments. *Chem Eng News 73*:32–42.

Ausubel FA, Brent R, Kingston RE, Moore DD, Seidman JG, Smith JA, Struhl K, eds. 1990. *Current protocols in molecular biology*. New York: Green Publishing and Wiley-Interscience.

Baker EN, Hubbard RE. 1984. Hydrogen bonding in globular proteins. *Prog Biophys Mol Biol 44*:97–179.

Bax A, Davis DG. 1985. MLEV-17-based two-dimensional homonuclear magnetization transfer spectroscopy. *J Magn Reson 65*:355–360.

Bax A, Ikura M, Kay LE, Torchia DA, Tschudin R. 1990. Comparison of different modes of two-dimensional reverse-correlation NMR for the study of proteins. *J Magn Reson 86*:304–318.

Bax A, Ikura M, Kay LE, Zhu G. 1991. Removal of F_1 baseline distortion and optimization of folding in multidimensional NMR spectra. *J Magn Reson 91*:174–178.

Blake PR, Park JB, Bryant FO, Aono S, Magnuson JK, Eccleston E, Howard JB, Summers MF, Adams MWW. 1991. Determinants of protein hyperthermostability: Purification and amino acid sequence of rubredoxin from the hyperthermophilic archeabacterium *Pyrococcus furiosus* and secondary structure of the zinc adduct by NMR. *Biochemistry 30*:10885–10895.

Blake PR, Park JB, Zhou ZH, Hare DR, Adams MWW, Summers MF. 1992. Solution-state structure by NMR of zinc-substituted rubredoxin from the marine hyperthermophilic archeabacterium *Pyrococcus furiosus*. *Protein Sci 1*:1508–1521.

Bodenhausen G, Ruben D. 1980. Natural abundance nitrogen-15 NMR by enhanced heteronuclear spectroscopy. *Chem Phys Lett 69*:185–189.

Brown SC, Weber PL, Mueller L. 1988. Toward complete ^{1}H NMR spectra in proteins. *J Magn Res 77*:166–169.

Day MW, Hsu BT, Joshua-Tor L, Park JB, Zhou ZH, Adams MWW, Rees DC. 1992. X-ray crystal structures of the oxidized and reduced forms of rubredoxin from the marine hyperthermophilic archaebacterium, *Pyrococcus furiosus*. *Protein Sci 1*:1494–1507.

Eidsness MK, O'Dell SE, Kurtz DM Jr, Robson RL, Scott RA. 1992. Expression of a synthetic gene coding for the amino acid sequence of *Clostridium pasteurianum* rubredoxin. *Protein Eng 5*:367–371.

Elkin CJ. 1995. Thermostability comparison of rubredoxin from *Clostridium pasteurianum* and *Pyrococcus furiosus* by site-directed mutagenesis [thesis]. Athens, Georgia: The University of Georgia.

Fesik SW, Zuiderweg ERP. 1988. Heteronuclear three-dimensional NMR spectroscopy. A strategy for the simplification of homonuclear two-dimensional NMR spectra. *J Magn Reson 78*:588–593.

Hirel PH, Schmitter JM, Dessen P, Fayat G, Blanquet S. 1989. Extent of N-terminal methionine excision from *Escherichia coli* proteins is governed by the side-chain length of the penultimate amino acid. *Proc Natl Acad Sci USA 86*:8274–8251.

Jeener J, Meier BH, Bachmann P, Ernst RR. 1979. Investigation of exchange processes by two-dimensional NMR spectroscopy. *J Chem Phys 71*: 4546–4533.

Johnson BH, Hecht MH. 1994. Recombinant proteins can be isolated from *E. coli* cells by repeated cycles of freezing and thawing. *Bio/Technology 12*:1357–1360.

Kissinger CR, Sieker LC, Adman ET, Jensen LH. 1991. Refined crystal structure of ferredoxin II from *Desulfovibrio gigas*. *J Mol Biol 219*:693–715.

Lovenberg W, Walker MN. 1978. Rubredoxin. *Methods Enzymol 53*: 340–346.

Mathieu I, Meyer J, Moulis JM. 1992. Cloning, sequencing and expression in *Escherichia coli* of the rubredoxin genes from *Clostridium pasteurianum*. *Biochem J 285*:255–262.

Marion D, Driscoll PC, Kay LE, Wingfield PT, Bax A, Gronenborn AM, Clore MG. 1989a. Overcoming the overlap problem in the assignment of ^{1}H NMR spectra of larger proteins by use of 3-D heteronuclear ^{1}H-^{15}N Hartman-Hahn multiple-quantum coherence and nuclear Overhauser-multiple-quantum coherence spectroscopy: Application to interleukin 1β. *Biochemistry 28*:6150–6156.

Marion D, Ikura M, Tschudin R, Bax A. 1989b. Rapid recording of 2D NMR spectra without phase cycling. Application to the study of hydrogen exchange in protein. *J Magn Reson 85*:393–399.

Marion D, Kay LE, Sparks SW, Torchia DA, Bax A. 1989c. Three-dimensional heteronuclear NMR of ^{15}N-labeled protein. *J Am Chem Soc 111*:1515–1517.

Morris GA, Freeman R. 1978. Selective excitation in Fourier transform nuclear magnetic resonance. *J Magn Reson 29*:433–462.

Rance M, Sorensen OW, Bodenhausen G, Wagner G, Ernst RR, Wüthrich K. 1983. Improved spectral resolution in COSY ^{1}H NMR spectra of proteins via double quantum filtering. *Biochem Biophys Res Commun 117*: 458–479.

Rees DC, Lewis M, Lipscomb WN. 1983. Refined crystal structure of carboxypeptidase A at 1.54 Å resolution. *J Mol Biol 168*:367–387.

Sambrook J, Fritsch EF, Maniatis T. 1990. *Molecular cloning: A laboratory manual, 2nd ed*. Cold Spring Harbor, New York: Cold Spring Harbor Laboratory Press.

Shaka AJ, Lee CJ, Pines A. 1988. Iterative schemes for bilinear operator: Application to spin decoupling. *J Magn Reson 77*:274–293.

Sieker LC, Stenkamp RE, LeGall J. 1994. Rubredoxin in crystalline state. *Methods Enzymol 243*:203–216.

Srinivasan PR, Lichter RL. 1977. Nitrogen-15 nuclear magnetic resonance spectroscopy. Evaluation of chemical shift references. *J Magn Reson 28*:227–234.

States DJ, Haberkorn RA, Reuben DJ. 1982. A two-dimensional nuclear Overhauser experiment with pure absorption phase in four quadrants. *J Magn Reson 48*:741–751.

Studier WF, Rosenberg AH, Dunn JJ, Dubendorff JW. 1990. Use of T7 RNA polymerase to direct expression of cloned genes. *Methods Enzymol 185*:60–89.

Tabor S. 1990. Expression using the T7 RNA polymerase/promoter system. In: Ausubel FA, Brent R, Kingston RE, Moore DD, Seidman JG, Smith JA, Struhl K, eds. *Current protocols in molecular biology*. New York: Green Publishing and Wiley-Interscience. pp 16.2.1–16.2.11.

Watenpaugh KD, Sieker LC, Jensen LH. 1979. The structure of rubredoxin at 1.2 Å resolution. *J Mol Biol 131*:509–522.

Wüthrich K. 1986. *NMR of proteins and nucleic acids*. New York: John Wiley & Sons. pp 117–174.

Zeng Q, Smith ET, Kurtz DM Jr, Scott RA. 1995. Protein determinants of metal site reduction potentials. Site-directed mutagenesis studies of *Clostridium pasteurianum* rubredoxin. *Inorg Chim Acta*. Forthcoming.